Hindawi
Shock and Vibration
Volume 2019, Article ID 7692424, 12 pages
https://doi.org/10.1155/2019/7692424

Research Article

A Damage Constitutive Model of Red Sandstone under Coupling of Wet-Dry Cycles and Impact Load

Bin Du[1,2,3] **and Haibo Bai**[1]

[1]*State Key Laboratory for Geomechanics and Deep Underground Engineering, China University of Mining and Technology, Xuzhou 221116, Jiangsu, China*
[2]*Institute of Architectural Engineering Technology, Jiangsu Vocational Institute of Architectural Technology, Xuzhou, Jiangsu 221116, China*
[3]*Jiangsu Collaborative Innovation Center for Building Energy Saving and Construction Technology, Xuzhou, Jiangsu 221116, China*

Correspondence should be addressed to Haibo Bai; hbbai@126.com

Received 20 December 2018; Revised 26 February 2019; Accepted 16 April 2019; Published 9 May 2019

Academic Editor: Francesco Franco

In the engineering fields of mining, tunneling, slopes, and dams, rocks are usually subject to the coupling effect of impact load and wet-dry cycles. The deformation rule of rocks under the coupling effects is a symbolic mechanical property, which lays the foundation for the design and evaluation in the rock engineering. In this paper, the coupling damage was classified as mesodamage induced by wet-dry cycles and macrodamage induced by impact load, and the loading rate effect was considered as the load damage. Besides, a constitutive model of coupling damage was concluded based on Lemaitre's strain equivalent assumption. Consequently, the validity of the model was verified by a series of dynamic compression tests of red sandstone. Results indicated that the proposed damage constitutive model can definitely describe the dynamic stress-strain curves of red sandstone after wet-dry cycles and impact load. The evolution of coupling damage curves showed that wet-dry cycle damage plays a dominant role in the elastic deformation stage, while the yield failure stage is controlled by the load damage in which the loading rate cannot be ignored. Parametric study was also performed to analyze the effect of parameters on dynamic stress-strain curves. The proposed mode has the simple and reliable operation with few parameters and can efficiently predict the long-term deformation behavior of rocks subject to multiple wet-dry cycles.

1. Introduction

Due to periodical moisture changes caused by the ground water level, rainfall, or other reasons, rocks are usually subject to cyclic wet-dry cycles treatment in various areas such as mining, tunneling, slopes, and dams. As a typical weathering, wet-dry cycles lead to rock deterioration, posing a threat to the safety and stability of rock engineering [1–4]. Therefore, the study of physical and mechanical properties of rocks against wet-dry cycles is vitally important.

Recently, the effect of wet-dry cycles on physical and mechanical properties of rock materials has been emphasized in the relevant studies. In terms of physical properties, the density, porosity, slake durability, and P-wave velocity have been studied. For instance, the surface roughness, bulk density, and porosity of mudrock after 3 wet-dry cycles were measured by Pardini et al. [1]. It was concluded that the porosity increases with the increasing wet-dry cycles, while the surface roughness and bulk density are independent of wet-dry cycles. Özbek [3] carried out a systematic experiment and analyzed the specific gravity, apparent porosity, unit weight, water absorption by weight, P-wave velocity, and slake durability index of ignimbrite samples subject to wet-dry cycles. They claimed that cyclic wet-dry treatments have different negative effects on the physical parameters mentioned above, and the sensibility to wet-dry cycles depends on the mineral type of rocks. Zhou et al. [5] concluded that the porosity and water absorption of sandstone increase

with the increasing wet and dry cycles, while SDI, density, and P-wave velocity decrease. In terms of mechanical properties, uniaxial compressive strength, shear strength, tensile strength, fracture toughness, and elastic modulus have been studied. Liu et al. [6] obtained that the elastic modulus and compressive strength of shaly sandstone decrease with the increasing wet-dry cycles, and the deterioration degree increases with the increase of wet-dry cycles. Hale and Shakoor [7] reported that the process of wet-dry treatment has no obvious effect on the unconfined compressive strength of sandstones. Khanlari and Abdilor [8] measured the uniaxial compressive strength of five different types of sandstone treated by wet-dry cycles. They found that there is no significant correlation between uniaxial compressive strength and wet-dry cycles, resulting from a variety of reasons, such as the mineral composition, anisotropic features, original defects, and artificial errors. Zhao et al. [9] reported that cyclic wet-dry cycles cannot reduce the tensile strength of sandstone with low clay mineral content because the weak performance mainly arises from the chemical and corrosive deterioration. Hua et al. [10] concluded that both the fracture toughness and tensile strength decrease with the increase of wet-dry cycles.

The existing studies are mainly concentrated on static tests, while the effect of cyclic wet-dry on the dynamic response of rocks has not been clearly studied. In the practical rock engineering such as drilling, tunneling, and blasting, rocks may be broken under dynamic load induced by impact operation. After the cyclic wetting and drying treatment, rock samples are more close to the actual stress state of rock materials in geotechnical engineering [11–13]. Therefore, it is meaningful to investigate the dynamic properties of rocks subject to cyclic wet-dry cycles. Zhou et al. [5, 12] conducted a range of impact tests to investigate the dynamic tensile strength and dynamic compressive strength of sandstone after wet-dry cycles. It was concluded that both dynamic compression and tensile strength decrease with the increasing wet-dry cycles. According to the test results, a decay model was proposed to forecast the long-term dynamic tensile strength. However, the damage constitutive behaviors under the coupling effect of wet-dry cycles and dynamic load have not been studied yet. In natural environments, rock materials may subject to lots of wet-dry cycles, which could last for several years, and it is unpractical to obtain the dynamic properties of rock after every given wet-dry cycles via experiments. Thus, a damage constitutive model considering the loading rate and number of wet-dry cycles should be developed to predict the long-term mechanical properties of rock, which could be obtained without experiments.

To characterize the evolution of dynamic stress-strain curves of rock under the coupling effect of wet-dry cycles and impact load, a damage constitutive model is developed from both the macro- and microscale in this paper. Based on Lemaitre's strain equivalence hypothesis, the coupling damage variable is determined through the combination of wet-dry cycle damage and load damage. It should be noted that the loading rate is considered as the load damage. The evolution of coupling damage variable versus strain and parametric analysis of the model are discussed. In the end, the proposed model is verified through the comparison between measured and calculated stress-strain curves.

2. Statistical Damage Constitutive Model under the Coupling Effect of Wet-Dry Cycles and Load

To describe the stress-strain relationship of concrete, a multiscale damage constitutive model subject to the combined action of freeze-thaw cycles and load was proposed by Wang et al. [14] on the basis of Lemaitre's strain equivalence hypothesis. In this model, the damage caused by freeze-thaw cycles was considered as the microscopic damage, which was determined by the variation of elastic modulus. Meanwhile, load damage was considered as the macroscopic damage described by Weibull distribution function. The validity of the proposed model was verified by experiments. However, the loading rate effect was ignored in this model, especially within the scope of dynamic tests. In this study, considering the coupling effect of wet-dry cycles and dynamic load with varying loading rates, an improved damage constitutive model is proposed on the basis of Wang's model.

2.1. Damage Constitutive Relations of Red Sandstone under Wet-Dry Cycles and Load. The deterioration of red sandstone induced by wet-dry cycles is identified as the microscopic damage, and the damage caused by dynamic load is regarded as the macroscopic damage. It should be emphasized that the following analysis of coupling damage under wet-dry cycles and dynamic load all follow Lemaitre's hypothesis.

Figure 1 shows the superposition of the damage variable. It is clearly seen that the damage status induced by the coupling treatment equals to the sum of status caused by macroscopic and microscopic damage and then minus the original status without any damage. The relation of strain among the three statuses can be expressed as follows:

$$\varepsilon_{12} = \varepsilon_1 + \varepsilon_2 - \varepsilon_0. \tag{1}$$

When the stress remains the same, the relationship between stress and elastic modulus can be defined as follows:

$$\frac{\sigma}{E_{12}} = \frac{\sigma}{E_1} + \frac{\sigma}{E_2} - \frac{\sigma}{E_0}. \tag{2}$$

According to Lemaitre's strain equivalence hypothesis, the elastic modulus is defined as [15]

$$\begin{cases} E_{12} = E_0(1 - D_{12}), \\ E_1 = E_0(1 - D_1), \\ E_2 = E_0(1 - D_2). \end{cases} \tag{3}$$

From equations (1)~(3), D_{12}, defined as the coupling damage variable, can be expressed as follows [16, 17]:

$$D_{12} = 1 - \frac{(1 - D_1)(1 - D_2)}{1 - D_1 D_2}. \tag{4}$$

The damage variable D_{12} represents the coupling damage behavior under wet-dry cycles and load. On the one hand,

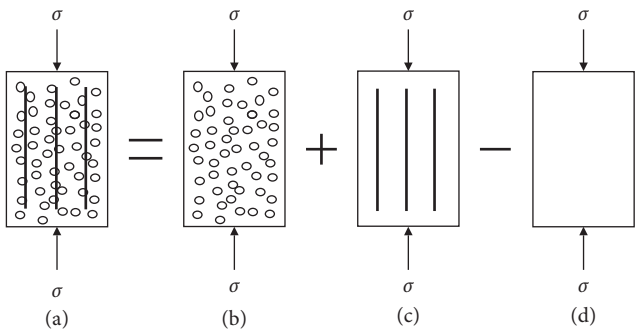

Figure 1: Superposition of coupling damage variable. Samples subject to (a) both macroscopic and mesoscopic damage, (b) only mesoscopic damage, (c) only macroscopic damage, and (d) and free of any damage. The damage variable, strain, and elastic modulus under stress are D_{12}, D_1, D_2, and D_0; ε_{12}, ε_1, ε_2, and ε_0; and E_{12}, E_1, E_2, and E_0, respectively.

when rocks are free of the wet-dry cycle, namely, $D_1 = 0$ and then $D_{12} = D_2$, unweathered rocks only show the load damage pattern under the stress. On the other hand, when rocks are only subject to wet-dry cycles, namely, $D_2 = 0$ and then $D_{12} = D_1$, the coupling damage variable equals to the macroscopic damage variable. Besides, with the increase of D_1 or D_2, the coupling damage variable always tends to increase, which is consistent with the actual situation. Accordingly, D_{12} reflects the actual evolution of damage subject to the coupling effect of wet-dry cycles and load. According to the theory of continuous damage, the constitutive relation of red sandstone under wet-dry cycles and dynamic load can be expressed as Lemaitre [18]:

$$\sigma = E(1 - D_{12})\varepsilon = E\varepsilon\frac{(1 - D_1)(1 - D_2)}{1 - D_1 D_2}. \tag{5}$$

2.2. Determination of Damage Variable

2.2.1. Damage Variable of Red Sandstone Subject to Wet-Dry Cycles. When the red sandstone is subject to cyclic wet-dry treatment, the mechanical properties of rocks have a varying deterioration, especially the elastic modulus. Thus, the damage caused by wet-dry cycles can be measured by the relative variation of the elastic modulus. Therefore, the wet-dry cycle damage variable of red sandstone is described as Huang et al. [19]:

$$D_1 = 1 - \frac{E_n}{E_0}, \tag{6}$$

where E_0 is the elastic modulus of the untreated specimen and E_n is the elastic modulus of the specimen after n cycles of wet-dry treatment.

2.2.2. Damage Variable of Red Sandstone Subject to Load. As a typical heterogeneous material, there are large numbers of uniform and randomly distributed internal defects in the rock (e.g., flaws, microvoids, grain boundaries, and weak medium) [20]. Before the establishment of the load damage evolution equation, the following assumptions should be addressed: (1) for each microelement, the evolution of strain and stress shows a linear relationship before failure and (2) the strength of the microelement satisfies the Weibull distribution, and the probability density function $p(\varepsilon)$ is defined as follows [21–24]:

$$p(\varepsilon) = \frac{m}{F_0}\left(\frac{\varepsilon}{F_0}\right)^{m-1}\exp\left[-\left(\frac{\varepsilon}{F_0}\right)^m\right], \tag{7}$$

where ε is the strain of red sandstone and F_0 and m represent distribution parameters of the model. When t is the broken microelements after a certain load, N is the total number of microelements, the damage variable D_2 is defined as follows:

$$D_2 = \frac{t}{N} = \frac{N\int_0^{\varepsilon} p(x)dx}{N} = 1 - e^{-(\varepsilon/F_0)^m}. \tag{8}$$

According to the Drucker–Prager failure criterion and extremum method, the distribution parameters F_0 and m of the model can be calculated as follows [25]:

$$m = -\frac{1}{\ln(\sigma_s/E\varepsilon_s)}, \tag{9}$$

$$F_0 = \varepsilon_s \sqrt[m]{m}, \tag{10}$$

where σ_s and ε_s are the peak stress and peak strain of red sandstone under the stress and E is the elastic modulus. The elastic modulus, which is calculated as the slope of stress-strain curves between 40% and 60% of the peak stress, can be approximately calculated by the following equation [26]:

$$E = \frac{\sigma_{0.6} - \sigma_{0.4}}{\varepsilon_{0.6} - \varepsilon_{0.4}}, \tag{11}$$

where $\sigma_{0.6}$ and $\sigma_{0.4}$ are 60% and 40% of peak strength, respectively, and $\varepsilon_{0.6}$ and $\varepsilon_{0.4}$ are 60% and 40% of peak strain, respectively.

When equation (10) is substituted into equation (8), the load damage variable is expressed as follows:

$$D_2 = 1 - e^{-(1/m)(\varepsilon/\varepsilon_s)^m}. \tag{12}$$

As discussed in Sections 2.1 and 2.2, the coupling damage variable is divided into two parts and then combined by equation (5). Based on this principle, D_1 can be calculated from the static compression test subject to different numbers of wet-dry cycles. Except for the basic variable ε, the others (ε_s, σ_s, E, and m) are all dependent parameters of loading rate and can be defined with the aid of the regression method. It is noted that the analysis of the above four parameters should be defined on the basis of dynamic compression tests on unweathered specimens.

3. Materials and Experiments

3.1. Specimen Preparation. The sampled rock was red sandstone taken from Linyi, Shandong province of China. According to the analysis of X-ray diffraction, the main mineral compositions of the red sandstone were quartz

(66.4%), feldspar (18.3%), calcite (8.6%), hematite (6.3%), and other mineral components (<0.5%), such as chlorite and illite. The density, uniaxial compression strength, P-wave velocity, and Poisson's ratio were 2478 kg/m^3, 74.2 MPa, 2598 m/s, and 0.24, respectively. Red sandstone was processed into cylindrical specimens for static compression tests (diameter: 50 mm; length: 100 mm) and dynamic compression tests (diameter: 50 mm, length: 25 mm). All the specimens were carefully polished to satisfy the standard recommended by International Society for Rock Mechanics (ISRM) [27]. The specimens were extracted from the same block with good petrographic uniformity and geometrical integrity. Moreover, ultrasonic tests were conducted to achieve the good homogeneousness. Red sandstone specimens were divided into five groups; namely, specimens were subject to 0, 5, 10, 15, and 20 cycles. To decrease the dispersion and ensure the validity of test data, at least three samples were tested under each condition, and the test data were averaged in this paper.

3.2. Cyclic Wetting and Drying Setup. Generally, two procedures are involved in an intact wet-dry cycle: the process from dry to the saturated state and the process from saturated to the dry state. Based on this principle, several methods were conducted to simulate the process of wet-dry cycles by researchers [28–31], while the uniform standard has not been formed. In this study, the wet-dry cycle was implemented by natural submerging and oven drying. For each wet-dry cycle, specimens were submerged into the purified water for 24 hours. Then, they were dried in an oven for 24 hours at a constant temperature of 60°C and cooled to the room temperature. The number of the wet-dry cycle for the untreated specimens was 0.

3.3. Testing Equipment. Dynamic tests were performed by a split Hopkinson pressure bar (SHPB) system with 50 mm diameter. As shown in Figure 2, the SHPB system includes a transmitted bar, an incident bar, and a striker bar, whose lengths are 1400 mm, 2400 mm, and 290 mm, respectively. All the bars are made of high strength 40Cr steel with an elastic modulus of 210 GPa and a density of 7800 kg/m^3. Two strain gauges are, respectively, pasted on the incident bar and transmitted bar to gather strain signals through a dynamic signal acquisition instrument when the striker bar is launched by the gas gun. The specimen is sandwiched between the incident bar and the transmitted bar. The received incident wave, reflected wave, and transmitted wave are expressed as ε_I, ε_R, and ε_T, respectively.

4. Experimental Results and Analysis

4.1. Results of Wet-Dry Cycles. Figure 3 shows the surface feature of red sandstone subject to different numbers of wet-dry cycles. It can be seen that there is no obvious flaw or defect on the surface, and the microdeterioration plays a leading role in the process of cycles.

According to test results of static compression and equation (11), the elastic modulus of red sandstone after 0, 5, 10, 15, and 20 wet-dry cycles are calculated as 6.29 GPa, 5.60 GPa, 5.23 GPa, 4.82 GPa, and 4.53 GPa, respectively. Then, the wet-dry damage variable is obtained by equation (6). The relation of D_1 with the number of wet-dry cycles is described in Figure 4. It is clear that the wet-dry damage D_1 increases with the increase of wet-dry cycles, and the increasing speed appears to be faster in the first cycle than that in the last wet-dry cycles. It can be fitted with exponential function in equation (13). The damage mechanism can be explained as follows: cycling wet-dry cycles not only lead to the dissolution of soft granules, resulting in the increase of microvoids, but also lead to the formation, expansion, and connection of microcracks. Therefore, the integrality of microstructure is weakened. With the increasing number of wet-dry cycles, irreversible damage induced by wet-dry cycles accumulates in the rock, resulting in degradation of physical and mechanical properties:

$$D_1 = 0.424 - 0.421e^{-0.053n}. \quad (13)$$

4.2. Results of the Dynamic Compression Test

4.2.1. Dynamic Stress Equilibrium. In this study, a pulse-shaping device is designed by a soft rubber sheet of 10 mm in diameter and 1 mm in thickness placed on the free end of the incident bar. This device has been widely used by many researches. Figure 5 shows the stress evolution of a typical dynamic compression test. It is found that the transmitted pulse almost equals to the sum of reflected pulse and incident pulse, namely, ($\varepsilon_T = \varepsilon_I + \varepsilon_R$). It suggests that the dynamic force balance on both ends of the specimen has been assessed successfully. In addition, the incident wave is shaped from a rectangular pulse to a ramp pulse, and thus, the axial inertial effect can be ignored [32–34]. For other specimens subject to this dynamic test, the dynamic force balance should be checked cautiously.

4.2.2. Dynamic Stress-Strain Curves. Based on 1-D wave theory, the dynamic stress-strain curves of specimen are subject to varying wet-dry cycles and loading rates, as shown in Figure 6. For each group with a certain number of wet-dry cycles, the dynamic tests were conducted under various loading rates which were controlled by the impact pressure of the gas gun varying from 0.25 MPa to 0.5 MPa. To achieve a better presentation, Figure 6 lists a few curves for each group. As illustrated in Figure 6, the dynamic stress-strain curves are influenced both by the number of wet-dry cycles and loading rate. Besides, there are some similar characteristics in the shape of curves; i.e., the compaction behavior is not obvious in the initial stage, and the elastic deformation stage lasts for a long time before the yielding of the specimen. When the wet-dry cycles remain unchanged, the dynamic compression stress (defined as the peak stress), dynamic elastic modulus, and peak strain all increase with the

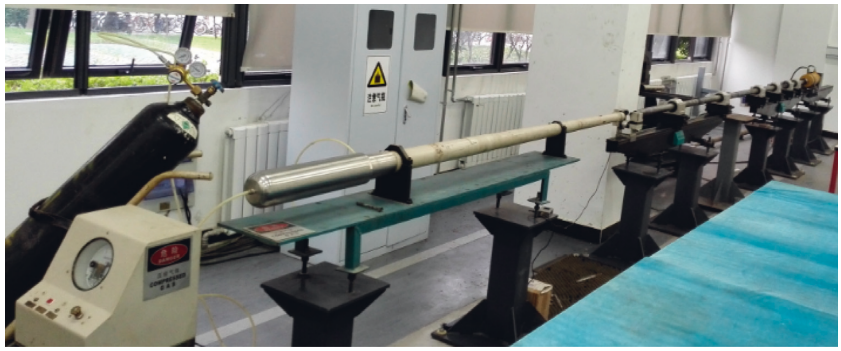

Figure 2: SHPB testing system.

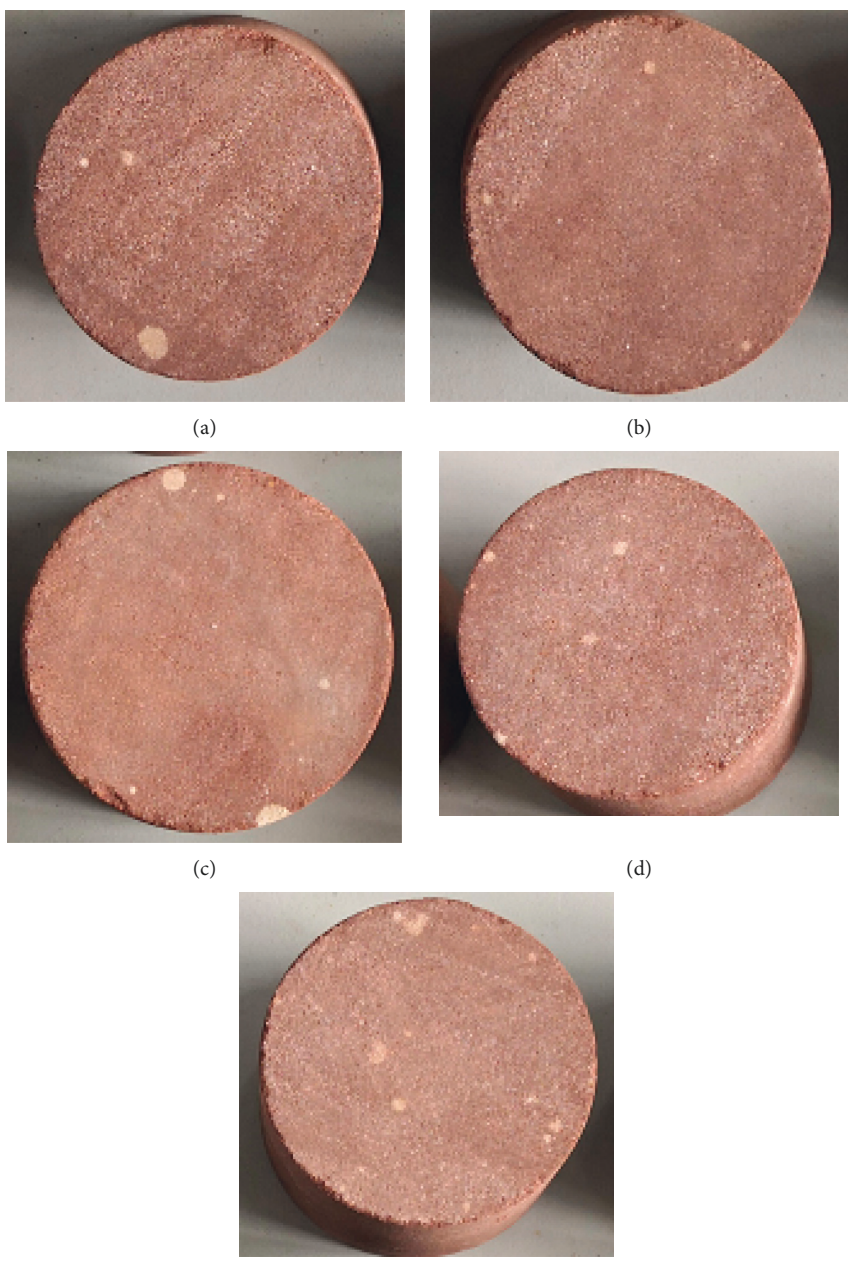

(a) (b) (c) (d) (e)

Figure 3: Surface features of specimens under different wet-dry cycles: (a) $n = 0$; (b) $n = 5$; (c) $n = 10$; (d) $n = 15$; (e) $n = 20$.

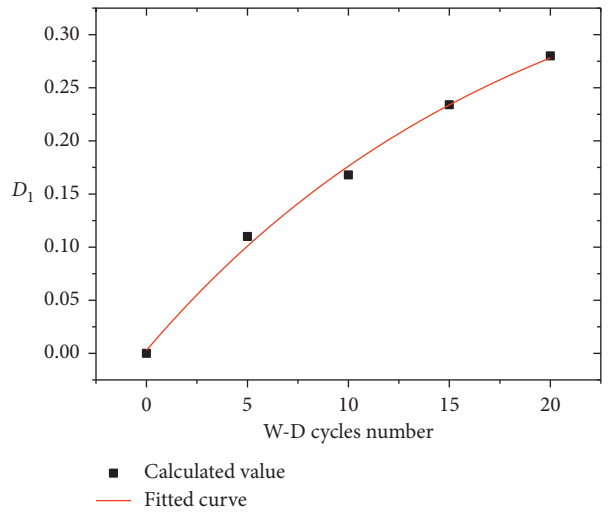

Figure 4: Variation of D_1 with the number of wet-dry cycles.

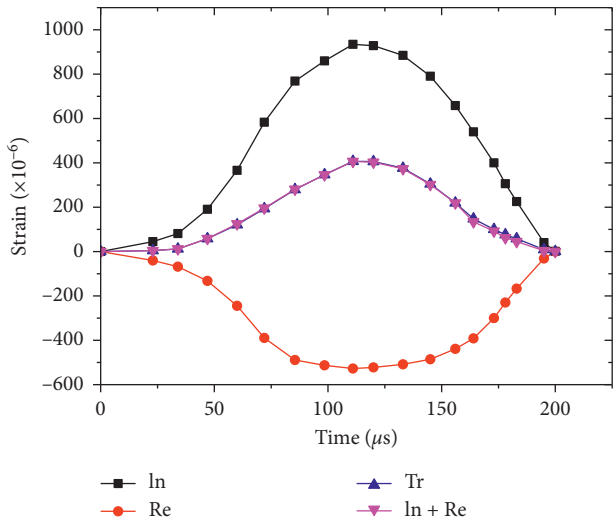

Figure 5: Dynamic stress equilibrium of the specimen.

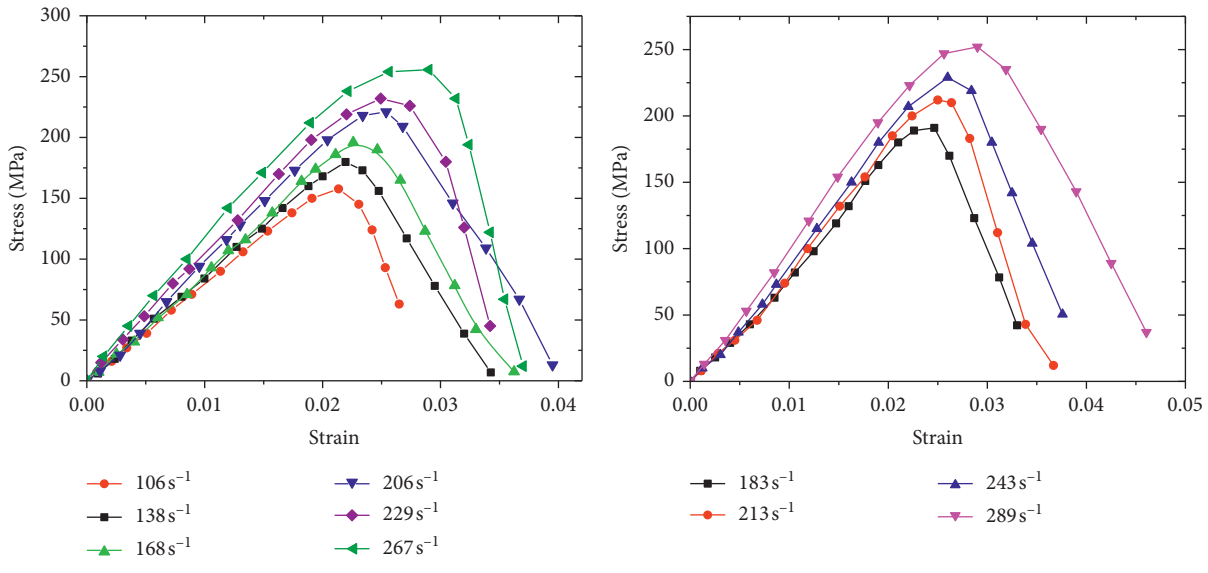

Figure 6: Continued.

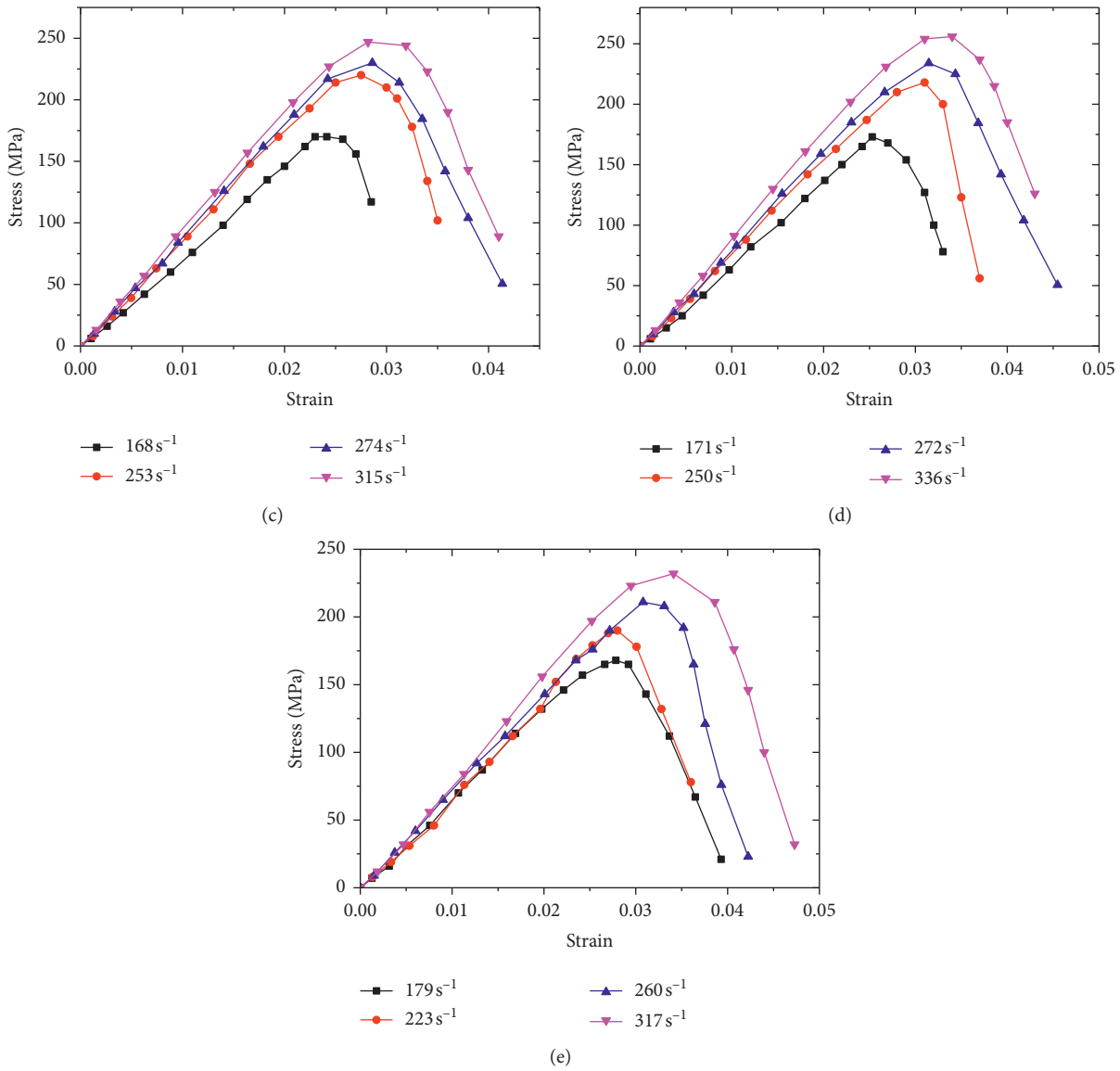

Figure 6: Dynamic stress-strain curves of specimens subject to (a) $n = 0$; (b) $n = 5$; (c) $n = 10$; (d) $n = 15$; (e) $n = 20$ wet-dry cycles.

increasing loading rate, regardless of the number of wet-dry cycles. Furthermore, except for the ascending branch, the descending branch of curves is also influenced by the loading rate.

4.3. Theoretical Verification. In Section 3.1, the damage (D_1) caused by wet-dry cycles is discussed, and the loading effect should take into account the remaining parameters, namely, dynamic elastic modulus (E), peak strain (ε_s), and dynamic compression stress (σ_s). Loading rate can be affected by these parameters.

Based on specimens free from the dynamic compression test, the measured parameters (E, ε_s, and σ_s) and calculated parameter (m) under different loading rates are listed in Table 1. Figure 7 illustrates the variation of parameters with the loading rate. The changing rules can be linearly fitted, as shown in the following equation:

Table 1: Parameters of the load damage model.

No.	$\dot{\varepsilon}(s^{-1})$	σ_s	ε_s	E (GPa)	m
DC0-1	106	157.8	0.0213	7.90	15.88
DC0-2	138	180.2	0.0220	8.76	14.74
DC0-3	168	195.7	0.0226	9.35	13.39
DC0-4	206	221.0	0.0244	9.79	12.94
DC0-5	229	232.2	0.0250	10.21	10.51
DC0-6	267	255.7	0.0272	10.86	10.17

$$\begin{cases} E = 6.224 + 0.0175\dot{\varepsilon}, \\ m = 19.80 - 0.037\dot{\varepsilon}, \\ \sigma_s = 95.37 + 0.602\dot{\varepsilon}, \\ \varepsilon_s = 0.017 + 3.627 \times 10^{-5}\dot{\varepsilon}. \end{cases} \quad (14)$$

By combining the equations mentioned above, the statistical constitutive model of red sandstone under the

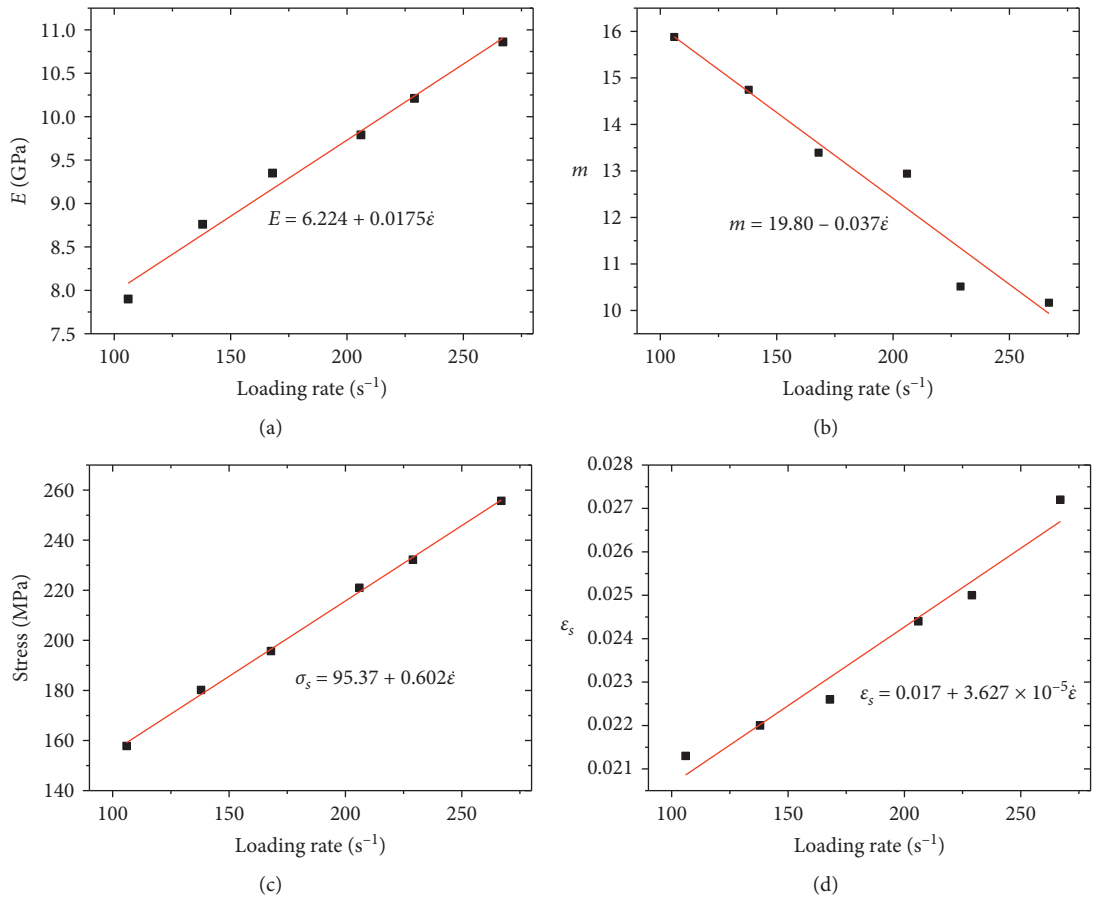

Figure 7: Variation of parameters versus loading. (a)–(d) The variation of E, m, σ_s, and ε_s versus loading rate, respectively.

coupling effect of the loading rate and wet-dry cycles can be obtained.

4.4. Coupling Damage Evolution of Red Sandstone. As shown in equation (12), the coupling damage variable is crucial for the evolution of deformation characteristics and determines the shape and changing laws of stress-strain curves. Concluded from equation (13), evolution curves of coupling damage under different numbers of wet-dry cycles at a certain loading rate (178 s^{-1}) are drawn in Figure 8. It can be seen that, there are mainly three stages in damage evolution curves, namely, the stable stage, rapid growth stage, and completing stage. No significant change can be observed with the increase of wet-dry cycles. During the first stage, the mesoscopic damage induced by wet-dry cycles plays a leading role, and the value of coupling damage almost equals to the wet-dry damage part. At this stage, the microvoids inside the rock begin to squeeze under the load, and the squeezing distance increases with the increasing number of wet-dry cycles, resulting in the serious deterioration. In the initiation, expansion, and coalescence of internal cracks, coupling damage sharply increases within a short range of strain, namely, between 0.0225 and 0.0325, and then increases to 1 practically. When the coupling damage is close to 1, the specimen is broken completely. The more the number of wet-dry cycles, the shorter the distance of the

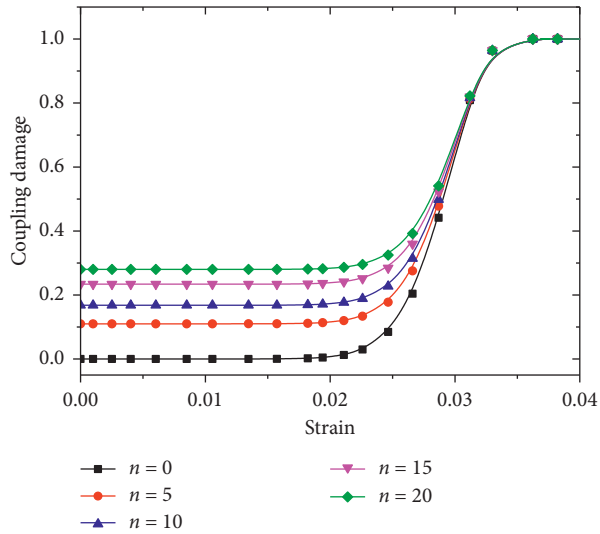

Figure 8: Damage evolution curves of red sandstone under different wet-dry cycles.

rapid growth stage. Figure 9 presents the coupling damage evolution of red sandstone subject to varying loading rates with 10 wet-dry cycles. The evolution process is similar to that in Figure 8 and can be classified into three stages, namely, two stable stages and a rapid growth stage. The

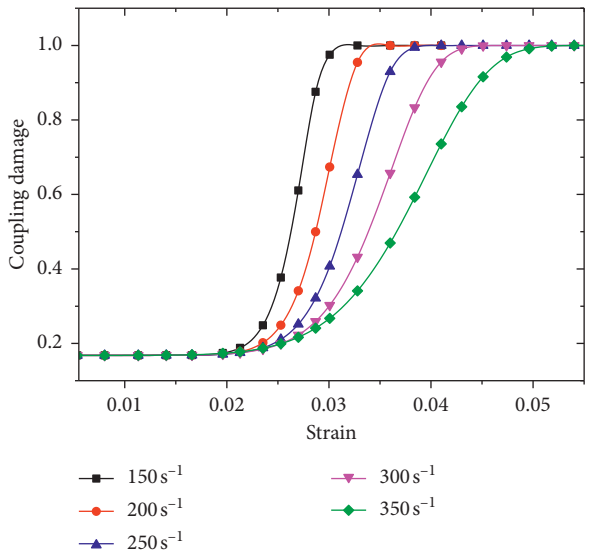

Figure 9: Damage evolution curves of red sandstone under different loading rates.

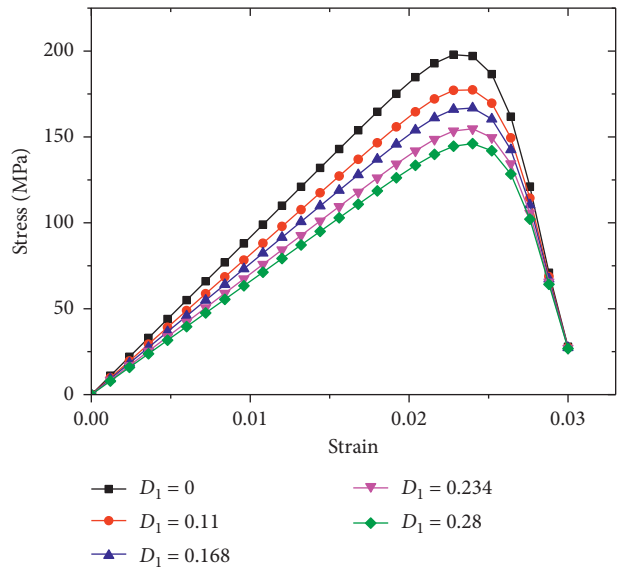

Figure 10: Effect of D_1 on stress-strain curves.

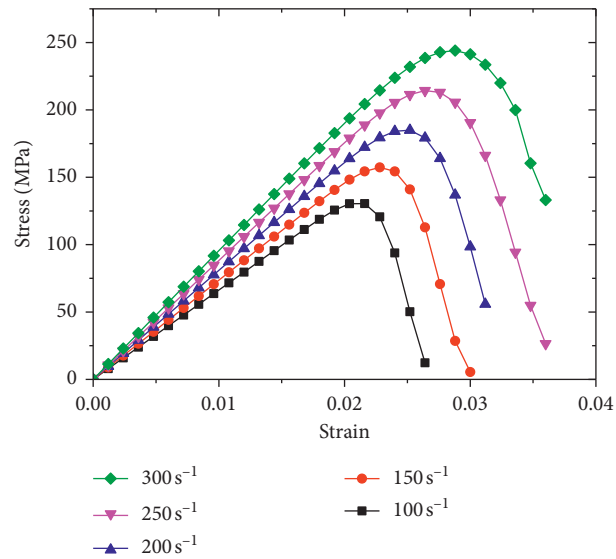

Figure 11: Loading rate effect on stress-strain curves.

critical strain of the first two stages is about 0.02. It is concluded that the starting point of the rapid growth stage is determined by the number of wet-dry cycles through the comparison of Figures 8 and 9. Besides, the more the cycles of wet-dry treatment, the bigger the strain of the starting point. Under the same wet-dry cycles, a larger strain period is required in the second stage when the loading rate is greater. In summary, the wet-dry damage plays a dominant role in the elastic deformation stage, while the yield failure stage is controlled by the load damage part, in which the loading rate cannot be ignored.

4.5. Parameter Sensitivity Analysis. To study the effect of two key parameters ($\dot{\varepsilon}$ and D_1) on the stress-strain curves, the parametric study was carried out based on the above fitting equation. The stress-strain curves at $\dot{\varepsilon} = 120$ are selected for the comparison. D_1 is taken as 0, 0.11, 0.168, 0.234, and 0.28, respectively, and five stress-strain curves are achieved, as shown in Figure 10. The peak strength and elastic modulus decrease with the adding up of D_1, while the peak strain is almost invariable. Figure 11 presents the stress-strain curves at $n = 5$ when $\dot{\varepsilon}$ is taken as 100, 150, 200, 250, and 300. It indicates that the peak stress, peak strain, and elastic modulus all increase with the increase of the loading rate.

4.6. Validation of the Statistical Damage Constitutive Model. To validate the rationality of the proposed model, red sandstone specimens after 5, 10, 15, and 20 wet-dry cycles were tested at the varying loading rate. Figure 12 shows the comparison of measured and calculated curves. As shown in Figure 12, the measured curves agree well with calculated curves in the ascending branch, while the consistency of the descending branch is not completely ideal. This is mainly caused by the change of the deformation characteristic in the descending branch. When the stress exceeds the peak point, the residual resistance of specimens after the destruction is mainly provided by the broken fragments rather than the rock itself. In fact, considering the practical value for rock engineering, the information provided by the ascending branch of stress-strain curves is more indispensable than that of the descending branch. Therefore, the proposed damage model can accurately reflect the mechanical response under the coupling effect of wet-dry cycles and dynamic load.

5. Conclusions

(1) The coupling damage caused by wet-dry cycles and impact load is classified as mesodamage induced by wet-dry cycles and macrodamage induced by impact load. According to Lemaitre's strain equivalent assumption, a damage constitutive model is proposed and validated by experiments.

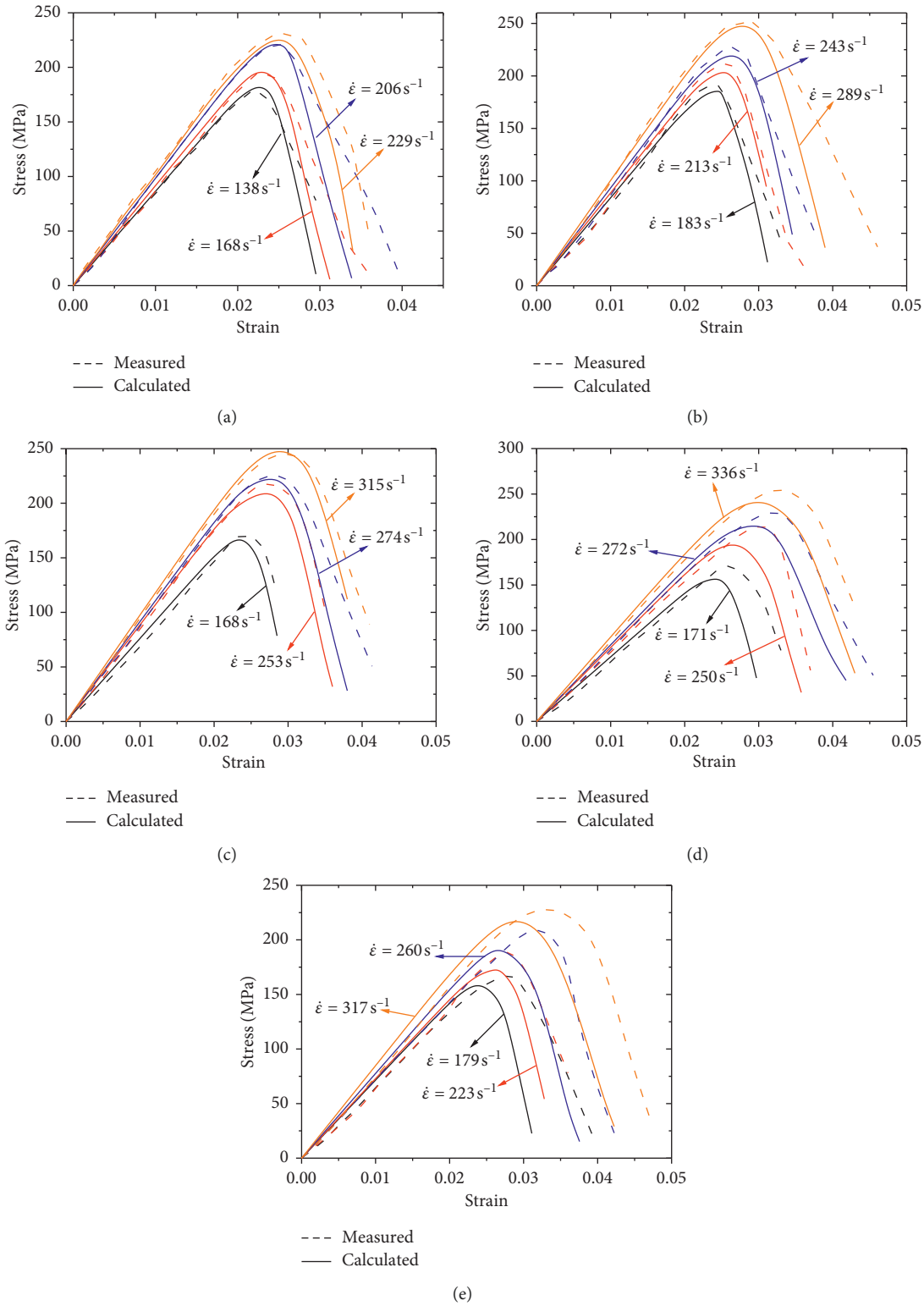

Figure 12: Comparison of measured and calculated stress-strain curves: (a) $n = 0$; (b) $n = 5$; (c) $n = 10$; (d) $n = 15$; (e) $n = 20$.

(2) The evolution of the coupling damage can be classified into three stages: stable stage, rapid growth stage, and completing stage. The critical strain between the stable stage and rapid growth stage is defined by the number of wet-dry cycles, and the critical strain between rapid growth and completing stage was controlled by the loading rate. Wet-dry cycle damage plays a key role in the elastic deformation stage, while the yield failure stage is controlled by the load damage when considering the loading rate.

(3) Parametric analysis shows that the peak strain is irrelevant to D_1 under a fixed loading rate, while the dynamic compression stress, elastic modulus, and peak strain tend to increase with the increasing loading rate when the number of wet-dry cycles remains unchanged. These analysis results agree well with the experiments.

Data Availability

The data used to support the findings of this study are partly included within the article, and the other data not included could be available from the corresponding author upon request.

Conflicts of Interest

The authors declare that they have no conflicts of interest.

Acknowledgments

The work was supported by the National Natural Science Foundation of China (51323004 and 51704281), the Major Issues of Natural Science Research in Jiangsu Higher Education Institutions (17KJA560002), the Natural Science Foundation of Jiangsu Higher Education Institutions (17KJB440002 and 18KJB480003), and the Doctor Special Research Fund of Jiangsu Collaborative Innovation Center for Building Energy Saving and Construct Technology (SJXTBS1701 and SJXTBS1705). The corresponding author would like to thank the financial support by State Key Laboratory for Geomechanics and Deep Underground Engineering, China University of Mining & Technology (SKLGDUEK1805).

References

[1] G. Pardini, G. V. Guidi, R. Pini, D. Regues, and F. Gallart, "Structure and porosity of smectitic mudrocks as affected by experimental wetting-drying cycles and freezing-thawing cycles," *Catena*, vol. 27, no. 3-4, pp. 149–165, 1996.

[2] D. Ma, M. Rezania, H.-S. Yu, and H.-B. Bai, "Variations of hydraulic properties of granular sandstones during water inrush: effect of small particle migration," *Engineering Geology*, vol. 217, pp. 61–70, 2017.

[3] A. Özbek, "Investigation of the effects of wetting-drying and freezing-thawing cycles on some physical and mechanical properties of selected ignimbrites," *Bulletin of Engineering Geology and the Environment*, vol. 73, no. 2, pp. 595–609, 2014.

[4] D. Ma, H. Duan, J. Liu, X. Li, and Z. Zhou, "The role of gangue on the mitigation of mining-induced hazards and environmental pollution: an experimental investigation," *Science of the Total Environment*, vol. 664, pp. 436–448, 2019.

[5] Z. Zhou, X. Cai, D. Ma et al., "Water saturation effects on dynamic fracture behavior of sandstone," *International Journal of Rock Mechanics and Mining Sciences*, vol. 114, pp. 46–61, 2019.

[6] X. Liu, M. Jin, D. Li, and L. Zhang, "Strength deterioration of a shaly sandstone under dry–wet cycles: a case study from the three gorges reservoir in China," *Bulletin of Engineering Geology and the Environment*, vol. 77, no. 4, pp. 1607–1621, 2018.

[7] P. A. Hale and A. Shakoor, "A laboratory investigation of the effects of cyclic heating and cooling, wetting and drying, and freezing and thawing on the compressive strength of selected sandstones," *Environmental and Engineering Geoscience*, vol. 9, no. 2, pp. 117–130, 2003.

[8] G. Khanlari and Y. Abdilor, "Influence of wet-dry, freeze-thaw, and heat-cool cycles on the physical and mechanical properties of upper red sandstones in central Iran," *Bulletin of Engineering Geology and the Environment*, vol. 74, no. 4, pp. 1287–1300, 2015.

[9] Z. Zhao, J. Yang, D. Zhang, and H. Peng, "Effects of wetting and cyclic wetting-drying on tensile strength of sandstone with a low clay mineral content," *Rock Mechanics and Rock Engineering*, vol. 50, no. 2, pp. 485–491, 2017.

[10] W. Hua, S. Dong, Y. Li, J. Xu, and Q. Wang, "The influence of cyclic wetting and drying on the fracture toughness of sandstone," *International Journal of Rock Mechanics and Mining Sciences*, vol. 78, pp. 331–335, 2015.

[11] D. Ma, X. Cai, Q. Li, and H. Duan, "In-situ and numerical investigation of groundwater inrush hazard from grouted karst collapse pillar in longwall mining," *Water*, vol. 10, no. 9, p. 1187, 2018.

[12] Z. Zhou, X. Cai, D. Ma, L. Chen, S. Wang, and L. Tan, "Dynamic tensile properties of sandstone subjected to wetting and drying cycles," *Construction and Building Materials*, vol. 182, pp. 215–232, 2018.

[13] D. Ma, X. Cai, Z. L. Zhou, and X. B. Li, "Experimental investigation on hydraulic properties of granular sandstone and mudstone mixtures," *Geofluids*, vol. 2018, Article ID 9216578, 13 pages, 2018.

[14] B. Wang, F. Wang, and Q. Wang, "Damage constitutive models of concrete under the coupling action of freeze-thaw cycles and load based on lemaitre assumption," *Construction and Building Materials*, vol. 173, pp. 332–341, 2018.

[15] D. Ma, X. X. Miao, H. B. Bai et al., "Impact of particle transfer on flow properties of crushed mudstones," *Environmental Earth Sciences*, vol. 75, no. 7, p. 593, 2016.

[16] H. Y. Liu, S. R. Lv, L. M. Zhang, and X. P. Yuan, "A dynamic damage constitutive model for a rock mass with persistent joints," *International Journal of Rock Mechanics and Mining Sciences*, vol. 75, pp. 132–139, 2015.

[17] Y. Liu and F. Dai, "A damage constitutive model for intermittent jointed rocks under cyclic uniaxial compression," *International Journal of Rock Mechanics and Mining Sciences*, vol. 103, pp. 289–301, 2018.

[18] J. Lemaitre, "A continuous damage mechanics model for ductile fracture," *Journal of Engineering Materials and Technology*, vol. 107, no. 1, pp. 83–89, 1985.

[19] S. Huang, Q. Liu, A. Cheng, and Y. Liu, "A statistical damage constitutive model under freeze-thaw and loading for rock and its engineering application," *Cold Regions Science and Technology*, vol. 145, pp. 142–150, 2017.

[20] G. Zhao, L. Xie, and X. Meng, "A damage-based constitutive model for rock under impacting load," *International Journal of Mining Science and Technology*, vol. 24, no. 4, pp. 505–511, 2014.

[21] W. Weibull, "A statistical distribution function of wide applicability," *Journal of Applied Mechanics*, vol. 18, pp. 293–297, 1951.

[22] H. M. Zhang and G. S. Yang, "Damage model and damage mechanical characteristics of loaded rock under freeze-thaw conditions," *Advanced Materials Research*, vol. 168–170, pp. 658–662, 2010.

[23] D. Ma, X. Miao, H. Bai et al., "Effect of mining on shear sidewall groundwater inrush hazard caused by seepage instability of the penetrated karst collapse pillar," *Natural Hazards*, vol. 82, no. 1, pp. 73–93, 2016.

[24] D. Ma and H. B. Bai, "Groundwater inflow prediction model of karst collapse pillar: a case study for mining-induced groundwater inrush risk," *Natural Hazards*, vol. 76, no. 2, pp. 1319–1334, 2015.

[25] D. K. Wang, S. M. Liu, J. P. Wei, H. L. Wang, and M. Peng, "Analysis and strength statistical damage constitutive model of coal under impacting failure," *Journal of China Coal Society*, vol. 41, pp. 3024–3031, 2016.

[26] T.-B. Yin, R.-H. Shu, X.-B. Li, P. Wang, and X.-L. Liu, "Comparison of mechanical properties in high temperature and thermal treatment granite," *Transactions of Nonferrous Metals Society of China*, vol. 26, no. 7, pp. 1926–1937, 2016.

[27] Y. X. Zhou, K. Xia, X. B. Li et al., "Suggested methods for determining the dynamic strength parameters and mode-I fracture toughness of rock materials," *International Journal of Rock Mechanics and Mining Sciences*, vol. 49, no. 1, pp. 105–112, 2012.

[28] K. Hall and A. Hall, "Weathering by wetting and drying: some experimental results," *Earth Surface Processes and Landforms*, vol. 21, no. 4, pp. 365–376, 1996.

[29] Z. Zhou, X. Cai, D. Ma, W. Cao, L. Chen, and J. Zhou, "Effects of water content on fracture and mechanical behavior of sandstone with a low clay mineral content," *Engineering Fracture Mechanics*, vol. 193, pp. 47–65, 2018.

[30] P. D. Sumner and M. J. Loubser, "Experimental sandstone weathering using different wetting and drying moisture amplitudes," *Earth Surface Processes and Landforms*, vol. 33, no. 6, pp. 985–990, 2008.

[31] M. L. Lin, F. S. Jeng, L. S. Tsai, and T. H. Huang, "Wetting weakening of tertiary sandstones-microscopic mechanism," *Environmental Geology*, vol. 48, no. 2, pp. 265–275, 2005.

[32] F. Dai, S. Huang, K. Xia, and Z. Tan, "Some fundamental issues in dynamic compression and tension tests of rocks using split Hopkinson pressure bar," *Rock Mechanics and Rock Engineering*, vol. 43, no. 6, pp. 657–666, 2010.

[33] Y. Xu and F. Dai, "Dynamic response and failure mechanism of brittle rocks under combined compression-shear loading experiments," *Rock Mechanics and Rock Engineering*, vol. 51, no. 3, pp. 747–764, 2018.

[34] H.-B. Du, F. Dai, Y. Xu, Y. Liu, and H.-N. Xu, "Numerical investigation on the dynamic strength and failure behavior of rocks under hydrostatic confinement in SHPB testing," *International Journal of Rock Mechanics and Mining Sciences*, vol. 108, pp. 43–57, 2018.